J Radioanal Nucl Chem (2013) 298:993–1003
DOI 10.1007/s10967-013-2497-8

A multi-method approach for determination of radionuclide distribution in trinitite

Christine Wallace · Jeremy J. Bellucci · Antonio Simonetti · Tim Hainley · Elizabeth C. Koeman · Peter C. Burns

Received: 21 January 2013 / Published online: 13 April 2013
© Akadémiai Kiadó, Budapest, Hungary 2013

Abstract The spatial distribution of radiation within trinitite thin sections have been mapped using alpha track radiography and beta autoradiography in combination with optical microscopy and scanning electron microscopy. Alpha and beta maps have identified areas of higher activity, and these are concentrated predominantly within the surficial glassy component of trinitite. Laser ablation-inductively coupled plasma mass spectrometry (LA-ICP-MS) analyses conducted at high spatial resolution yield weighted average $^{235}U/^{238}U$ and $^{240}Pu/^{239}Pu$ ratios of 0.00718 ± 0.00018 (2σ) and 0.0208 ± 0.0012 (2σ), respectively, and also reveal the presence of some fission (^{137}Cs) and activation products ($^{152,154}Eu$). The LA-ICP-MS results indicate positive correlations between Pu ion signal intensities and abundances of Fe, Ca, U and ^{137}Cs. These trends suggest that Pu in trinitite is associated with remnants of certain chemical components from the device and surrounding Trinity test-related structures at ground zero. In contrast, negative correlations between Pu ion signals and SiO_2 and K_2O contents were observed within the glassy matrix of trinitite. This LA-ICP-MS result was corroborated by combined back-scattered electron imaging and alpha radiography, and indicates that Pu was not incorporated into unmelted crystalline grains of precursor minerals (i.e., quartz-SiO_2 and K-feldspar-$KAlSi_3O_8$) present within the desert sand at the Trinity site. The results from this study indicate that the device-related radionuclides were preferentially incorporated into the glassy matrix in trinitite.

Keywords Trinitite · Nuclear forensics · Radionuclides · Fission and activation products · Laser ablation inductively coupled plasma mass spectrometry

Introduction

Nuclear proliferation and terrorism are arguably the gravest of threats to the security of any nation. The ability to decipher forensic signatures in post-detonation nuclear debris is essential, both to provide a deterrence and to permit a response to an incident. Impacted material obtained from historical nuclear tests offers a unique opportunity for nuclear forensics method development, as the radioactive components of the weapons have been documented. Therefore, results obtained in a forensic investigation from the latter are verifiable.

Post-detonation material from the Trinity test, the world's first nuclear explosion, provides an opportunity for forensic studies, as most of the government literature on the test has been declassified and samples are available from public and private collections. The Trinity test was conducted on July 16, 1945 at the White Sands Missile Range near Alamogordo, NM, and represented the first of over 1000 nuclear tests conducted by the United States between 1945 and 1992 [1]. The Trinity "Gadget" was an implosion-type fission device containing ~6 kg of "super-grade" ^{239}Pu [2, 3]. The device was detonated from atop a 30.5 m steel tower at 5:29:45 a.m. local time, generating an explosion equivalent to that from ~21 kt of TNT [4]. The Trinity test created a fireball with a height of 15.2–21.3 km

Electronic supplementary material The online version of this article (doi:10.1007/s10967-013-2497-8) contains supplementary material, which is available to authorized users.

C. Wallace (✉) · J. J. Bellucci · A. Simonetti · T. Hainley · E. C. Koeman · P. C. Burns
Department of Civil and Environmental Engineering and Earth Sciences, University of Notre Dame, Notre Dame, IN 46556, USA
e-mail: cwallac1@nd.edu; cmwallace2123@gmail.com

and a temperature of ~8430 K [4]. The explosion engulfed the device and components, as well as the tower and the surrounding desert sand. Radionuclides, including un-fissioned Pu, fission products, and neutron activation products were also entrained in the cloud. When the debris re-solidified, it formed a layer of glassy material known as "trinitite" with a radial extent of 370 m [5].

A two-step formation mechanism has been proposed for trinitite [6, 7]: (1) formation of molten glass both on the ground and in the mushroom cloud, and (2) subsequent incorporation of solid material (non-molten mineral phases, metal, and droplets) raining down from the cloud on the upper surface of this solidifying glass. Of importance in relation to the forensic analysis of trinitite's glass matrix is the fact that the arid conditions of New Mexico's desert have likely prevented mobilization and leaching of long-lived radionuclides [2]; these include remnants of Pu fuel, fission products, and neutron activation products.

Several previous studies of trinitite have focused on radiochemical analysis [2, 8, 9]. Recently, several studies have highlighted the importance of examining trinitite at the micron scale for forensic purposes [6, 10, 11]. To date, an investigation describing the spatially resolved distribution of radionuclides within trinitite is lacking; however, given its heterogeneous nature at the micron scale, spatial resolution is deemed of utmost importance for understanding dispersion of radionuclides during a nuclear explosion. Hence, the purpose of this study is to investigate the distribution of radionuclides via methodologies that provide reasonably rapid and quasi non-destructive analyses of trinitite.

Remnants of Pu fuel

The Pu used in the Trinity device was produced at the Hanford site, with the natural U fuel being subjected to extremely short irradiation time as a result of the urgency during the Manhattan Project era [3]. During irradiation, ^{239}Pu is created via neutron capture on ^{238}U (creating ^{239}U), followed by two successive β-decays. During this process, ^{240}Pu and ^{241}Pu are also produced in situ by neutron capture on ^{239}Pu, with longer irradiation times resulting in a higher ^{240}Pu and ^{241}Pu content. The extremely low burn-ups used to produce the Pu fuel for the Trinity device resulted in ^{239}Pu that was nearly isotopically pure, as higher Pu isotopes did not have time to accumulate. Sublette estimated the original (pre-detonation) ^{240}Pu content of the Gadget to be ~0.9–1.0 %, with only trace amounts of other isotopes [12]. The Trinity device contained a total of 6 kg of Pu; based on Glasstone and Dolan's estimate of 1.45×10^{23} fissions occur per kiloton of yield [13], only 1.2 kg of ^{239}Pu were fissioned in the explosion [14]. It is assumed that the remaining ~4.8 kg of Pu did not fission and was consequently dispersed in the explosion.

Past studies of trinitite have documented the presence of ^{239}Pu [2, 6, 8, 11], as well as ^{238}Pu, ^{240}Pu, ^{241}Pu, and ^{241}Am [2, 6]. ^{238}Pu, ^{240}Pu, and ^{241}Pu could have been created during reactor irradiation via (n, 2n), (n, γ), and (2n, γ) reactions, respectively. However, it is more likely that these isotopes were actually produced during the explosion, due to the high purity of the original fuel [2]. ^{241}Am is present as a β-decay product of ^{241}Pu, which has a half-life of 14.3 years. Consequently, ^{241}Am has accumulated in trinitite since 1945 from the decay of ^{241}Pu [2, 6, 8].

Uranium

Natural uranium in trinitite may originate from two sources. Firstly, uranium is indigenous in mineral phases found within the desert sand at the Trinity site, including zircon, monazite, and apatite [10]. Additionally, the Gadget contained a 120-kg tamper composed of natural uranium, which functioned to avert a premature disassembly of the Pu core and to restrict initial movement of neutrons [15]. The tamper was dispersed in the explosion and incorporated into the melt material. Semkow (2006) [15] reported that ~30 % of the Gadget's explosive yield resulted from fission of ^{235}U within the tamper, and fission product ratios determined via gamma spectroscopy are consistent with fission of both ^{239}Pu and ^{235}U [8]. As a result, it is possible that ^{235}U/^{238}U ratios in trinitite will be slightly lower than natural.

Fission products

The Trinity test was conducted over six decades ago, and consequently only fission products with sufficiently long half-lives should still be detectable. For example, ^{137}Cs ($t_{1/2}$ = 30.17 years) is formed from the beta decay of short-lived fission products ^{137}Xe and ^{137}I, whereas ^{90}Sr ($t_{1/2}$ = 28.8 years) is derived from the short-lived ^{90}Rb. ^{90}Sr and ^{137}Cs have cumulative fission yields of 2.17 and 6.76 % from the fission of ^{239}Pu, respectively [16].

Neutron activation products

Upon detonation, the Pu core of the Gadget initiated a neutron flux that caused neutron activation of both device components and the surrounding sand. Previous studies have documented the presence of ^{60}Co, ^{133}Ba, ^{152}Eu, and ^{154}Eu in trinitite [2, 8]. ^{60}Co is derived from the (n, γ) reaction of ^{59}Co, which was present in the steel tower. Similarly, ^{133}Ba is produced via (n, γ) on ^{132}Ba, which

originated from the explosive lens system in the Gadget and in mineral phases, such as barite, within the desert sand [10]. ^{152}Eu and ^{154}Eu are neutron activation products of ^{151}Eu and ^{153}Eu, respectively. These isotopes are also present naturally in the desert sand at ground zero.

Major and trace elements

The major and trace element composition of trinitite is variable and reflects both natural and anthropogenic components [10]. In addition to the Pu and U components of the Trinity "Gadget", the device consisted of several concentric "shells" [15]. At the center of the Gadget was an initiator composed of ^{210}Po and Be, which served as a source of neutrons to begin the fission chain reaction upon activation [15]. Surrounding the initiator were two hemispheres of subcritical Pu, which were encased by the uranium tamper [15]. The other concentric layers consisted of a boron absorber, an aluminum pusher, and implosion system encased in a dural shell [15]. The implosion system consisted of conventional explosives, including Baratol (75 % $Ba(NO_3)_2$ and 25 % TNT) and an explosive containing 60 % RDX, 39 % TNT, and 1 % wax [15]. Upon detonation, these components were vaporized along with the blast tower, wiring, and electronics. Therefore, trinitite could contain signatures from any of these anthropogenic sources; for example, anomalous (i.e., higher than the geological background) Cu (and Pb) abundances resulting from the incorporation of wiring, or elevated Fe (and Co) contents originating from the melting of the blast tower.

Experimental methods

Samples and bulk analyses

The 14 Trinitite samples used in this study were purchased from the Mineralogical Research Corporation (www.minresco.com). Prior to analysis, each sample was photographed and weighed. An extensive gamma spectroscopic study [8] was conducted on bulk samples for comparison to results obtained by micro-analytical techniques, such as those reported here. Samples were subsequently cut and polished into thin sections with a thickness of 70–100 μm.

Imaging

Thin sections of trinitite were mapped using optical microscopy and scanning electron microscopy (SEM). Optical maps were generated in plane-polarized light using a petrographic microscope equipped with a digital camera. SEM analyses were performed at the University of Notre Dame Integrated Imaging Facility using a EVO 50 LEO Environmental SEM (Carl Zeiss). This instrument is equipped with both secondary electron and backscatter electron (BSE) detectors. An accelerating voltage of 30 kV and magnifications of 100–200× were used for these measurements. Prior to analysis, thin sections were mounted onto SEM stubs with conductive carbon tape and sputtered with Ir to a thickness of ~5 nm. Samples were imaged in BSE mode in order to detect relative differences in chemical composition. Compositional maps of entire thin sections were generated by merging adjacent BSE images in Adobe Photoshop. Individual phases (minerals, glass) within each sample were examined for elemental abundances semi-quantitatively using energy dispersive spectroscopy (EDS).

Alpha track radiography

CR-39 plastic detectors were used to record alpha tracks from trinitite thin sections. The samples were held in tight contact with the detectors for 7–10 days. Subsequently, the CR-39 detectors were etched in 6.25 M NaOH at 98 °C for 4 hours to reveal the alpha tracks. After the detectors were removed from the etching solution, they were rinsed in distilled water and neutralized for 30 min in 2 % glacial acetic acid. The plastic was then optically imaged with a light microscope to determine the areas of the sample that contain the highest alpha activity. Because the alpha-emitting radionuclides in trinitite are not uniformly distributed, this allowed for alpha-rich areas to be mapped prior to analysis with electron microprobe and LA-ICP-MS.

Beta radiography

Trinitite thin sections were placed two inches apart on Fujifilm BAS-SR2025 imaging plates and inserted into a lead cassette. Mylar film was placed between the samples and plates to avoid contamination of the plates. After 72 h of exposure, the plates were scanned with a Fujifilm BAS-5000 Image Reader, and images were obtained using Image Reader software. The results of these analyses were compared to alpha radiographs and used to identify areas of high β activity prior to microprobe and LA-ICP-MS analyses.

Electron microprobe

Major element analyses were completed at the University of Chicago using a Cameca SX-50 electron microprobe. Standardization was conducted using the following well-characterized in-house standards: olivine (Fe, Mg, Mn), albite (Na), anorthite (Ca, Al), asbestos (Si), microcline

(K), and rutile (Ti). Relative internal uncertainties (2σ mean) are based on counting statistics, and are ≤2 % for SiO_2, Al_2O_3, and CaO; ≤5 % for FeO, Na_2O, and K_2O; and ≤10 % for MnO, MgO, and TiO_2.

LA-ICP-MS

A total of 144 ICP-MS analyses were conducted at the MITERAC ICP-MS facility (University of Notre Dame) using a New Wave Research UP-213 laser ablation unit coupled to a ThermoFinnegan Element2 sector-field high resolution (HR)-ICP-MS. A 60-s background collection of ion signals was performed with the laser on and shuttered, followed by a 60-s ion signal collection. Instrument settings and analytical conditions are listed in Table 1 and are similar to those defined in Chen and Simonetti (in press) [17]. Sample analyses were bracketed by analyses of NIST SRM 612 glass wafer to monitor instrument drift and evaluate possible spectral interferences. All ion signals were measured in low mass resolution mode (mass/Δmass ≈300) due to the low concentrations (at ppt level) of the radionuclides.

All isotopic ratios were calculated using the background subtracted, average counts per second for each isotope measured. Internal uncertainty was calculated using Poisson's counting statistics, and the external reproducibility (i.e., relative standard deviation) associated with concentration determinations by LA-ICP-MS typically varies between 5 and 10 % (at the 2σ level). For measurement of Pu, formation of UH^+ was minimized using dry plasma and optimization of the ICP-MS instrument [18, 19]. The NIST SRM 612 wafer does not contain any Pu and consequently none of the standard analyses conducted in this study recorded detectable Pu ion signals. Alpha track radiography maps were used to guide laser ablation spot placement, with analyses being conducted in the areas of highest activity. Typically laser spots were placed at a distance of at least 250–500 μm apart. In some samples with high surface activity, transects were conducted with a spacing of ~500 μm between spots. Additionally, spot analyses were collected in areas of the samples where little or no alpha activity was revealed by radiography, and consequently ion signals at masses 239 or 240 were not detected.

The fission product ^{137}Cs and activation products ^{152}Eu and ^{154}Eu were detected via LA-ICP-MS and are reported using δ-notation; the latter is used for reporting stable isotope ratios of light elements (e.g., C, O, N). The presence of isobaric interferences at masses 137, 152, and 154 (Table 2) does not readily permit for the calculation of absolute elemental abundances (in ppm) for these elements. Evaluation of isobaric interferences at the masses of interest (e.g., 152 and 154; Table 2) was accomplished by comparison of calculated ratios, based on the total ion signals measured, to those for the natural abundance values of isotopes of Sm (152, 154), Gd (152, 154, 160), and Tb (160, 163). For example, the "true" ion signals of ^{152}Sm and ^{154}Sm were calculated based on natural atomic abundances of Sm and measurement of the interference-free ^{149}Sm ion signal. Consequently, isotope ratios of interest characterized by elevated values relative to both those recorded in the NIST SRM 612 analyses and natural abundance ratios were interpreted as enriched in parent and or daughter radioisotopes at that mass (as beta decay does not change mass number). Calculation of δ values (in ‰) was performed using the following equation:

$$\delta^{a}X = \left({}^{a}R_{\text{sample}} - {}^{a}R_{\text{standard}} / {}^{a}R_{\text{standard}}\right) \times 1000.$$

Ion signal intensities at mass 137 were measured relative to those recorded for ^{138}Ba. Ion signals measured at masses

Table 1 Analytical settings

Cameca 1 Electron microprobe[a]	
Accelerating voltage	15 kv
Beam size	15 mm
Beam current	35 nA
Thermofinnigan element 2 HR-ICP-MS[b]	
Forward power	1250 W
Reflected power	1 W
Cool gas (Ar)	16.61 L min^{-1}
Aux gas (Ar)	0.98 L min^{-1}
Sample gas (He)	0.6 L min^{-1}
Guard electrode	Enabled
Dwell time	8 ms
Samples per peak	1
Resolution	Low
Scan type	Escan
Th/ThO	<1 %
Isotopes measured	^{43}Ca[c], ^{53}Cr, ^{59}Co, ^{65}Cu, ^{71}Ga, ^{85}Rb, ^{86}Sr, ^{89}Y, ^{92}Zr, ^{93}Nb, ^{117}Sn, ^{133}Cs, ^{138}Ba, ^{139}La, ^{140}Ce, ^{141}Pr, ^{146}Nd, ^{147}Sm, ^{153}Eu, ^{160}Gd, ^{159}Tb, ^{163}Dy, ^{165}Ho, ^{166}Er, ^{169}Tm, ^{172}Yb, ^{175}Lu, ^{180}Hf, ^{181}Ta, ^{208}Pb, ^{232}Th, ^{238}U
New wave UP-213 laser ablation system	
Spot size (diameter)	55 um
Fluence	10 J cm^{-2}
Repetition	7 Hz

[a] University of Chicago

[b] University of Notre Dame

[c] Internal standard

Table 2 Isobaric mass interferences monitored and corrections applied

Mass	136	137	138	147	149	151	152	153	154	160	163
	Ba	Ba	Ba								
				Sm	Sm[b]	Eu	Sm	Eu	Sm		
							Gd		Gd	Gd	
							$^{136}Ba^{16}O$[a]		$^{138}Ba^{16}O$[a]	Dy	Dy

[a] Plasma oxide level (typically <1 %) was determined by comparison between total (measured) ion signal (cps) intensities for masses 152 and 154 and those calculated for 152Gd and 154Gd using natural atomic abundances of 160Gd and 163Dy based on laser ablation analyses of the NIST SRM 612 glass standard

[b] Calculated ion signal intensities (cps) for 152Sm and 154Sm were based on natural abundance isotope ratios for Sm using the measured, interference-free ion signal for 149Sm. Excesses in absolute ion signal intensities (cps) calculated on masses 152 and 154 for laser ablation analyses of trinitite are attributed to the presence of activation products 152Eu and 154Eu, respectively

152 and 154 were both compared relative to those for ^{149}Sm. Selection of the latter isotope was ideal due to the fact that there are no isobaric interferences from neighboring rare earth elements. Thus, results are reported as δ137/138, δ152/149, and δ154/149. δ152/149 and δ154/149 values were also filtered for isobaric interferences relating to the production of overlapping $^{136}Ba^{16}O$ (mass 152) and $^{138}Ba^{16}O$ (mass 154) oxides (Table 2). Oxide levels in the plasma were assessed based on discrepancies between calculated and measured total ion signals on masses 152 and 154 using natural abundances for isotopes of Gd, Sm, and Dy based on the NIST SRM 612 analyses (Table 2). Despite the calculated low oxide production levels in the plasma (<1.0 %), the latter are considered important given the Ba-rich nature of the trinitite samples (typically between ~100 and ~1000 ppm [10]).

Results

Bulk analyses

An extensive gamma spectroscopy study was conducted on 49 trinitite samples (Bellucci et al., in press) [8]. A typical trinitite gamma spectrum is shown in Fig. 1. The dominant anthropogenic radionuclides identified in all samples were ^{241}Am (59.5 keV), ^{152}Eu (122 keV), and ^{137}Cs (661.6 keV). Peaks from ^{154}Eu, ^{155}Eu, ^{133}Ba, and ^{239}Pu were also found in the spectra of some samples. These results provide a basis for comparison to the LA-ICP-MS data.

Distribution of alpha and beta activity

A typical optical map, along with the corresponding α- and β- radiographs, is shown in Fig. 2. Alpha activity is seen throughout the sample; however, it is mostly concentrated on the upper glassy surface in rounded, discrete clusters (1–3 mm in size). Beta activity is similarly concentrated on the upper surface of the sample, although it is significantly more diffuse than the alpha activity. Superposition of an alpha autoradiograph on a backscatter electron map reveals that alpha activity tends to be located in amorphous phases (as determined by examination via optical microscopy) between Si-rich grains (Fig. 3).

LA-ICP-MS

U and Pu

The U and Pu ratios calculated for the 144 spot analyses are shown in Fig. 4. These analyses yield a weighted mean [20] $^{235}U/^{238}U$ value of 0.00718 ± 0.00018 (2σ; $n = 138$ analyses—6 rejected), which is consistent with the 'natural' $^{235}U/^{238}U$ value. Pu was measured in areas of the trinitite thin sections that were characterized by high alpha activity, as determined by alpha track radiography. The average $^{240}Pu/^{239}Pu$ ratio determined is 0.0208 ± 0.0012 (2σ; $n = 137$ analyses—7 rejected), which is consistent with "supergrade" Pu and the $^{240}Pu/^{239}Pu$ ratios reported by Nygren and Douglas [21, 22].

Fission and neutron activation products

The presence of ^{137}Cs in bulk trinitite samples was verified via γ-spectroscopy (Fig. 1). However, this technique could not be used to identify ^{90}Sr because it is a pure β-emitter, and as such, does not emit characteristic γ-rays. We attempted to measure both ^{90}Sr and ^{137}Cs indirectly via LA-ICP-MS analyses and report their relative proportions as δ90/92 and δ137/138 values, respectively. For comparative purposes, Pu ion signal intensities were normalized to those for Zr since the latter is thought to originate strictly from the natural geological background; moreover, this normalization provides a means to compensate/adjust for differing ionization efficiencies during the laser ablation process, which are possibly matrix dependent. Calculated δ90/92 values revealed no detectable ^{90}Sr in any of the spots analyzed. Elevated δ137/138 values were determined

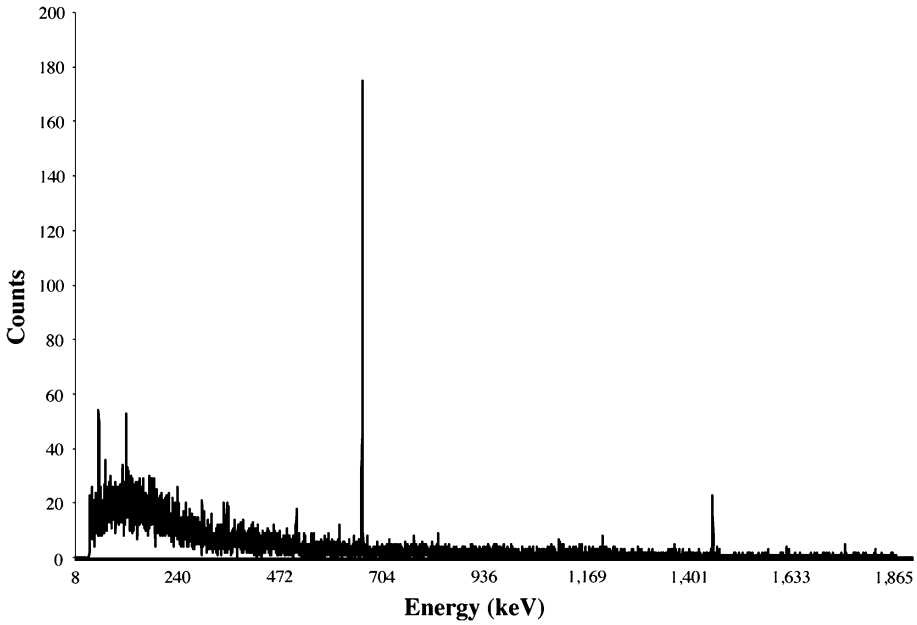

Fig. 1 A typical trinitite gamma spectrum

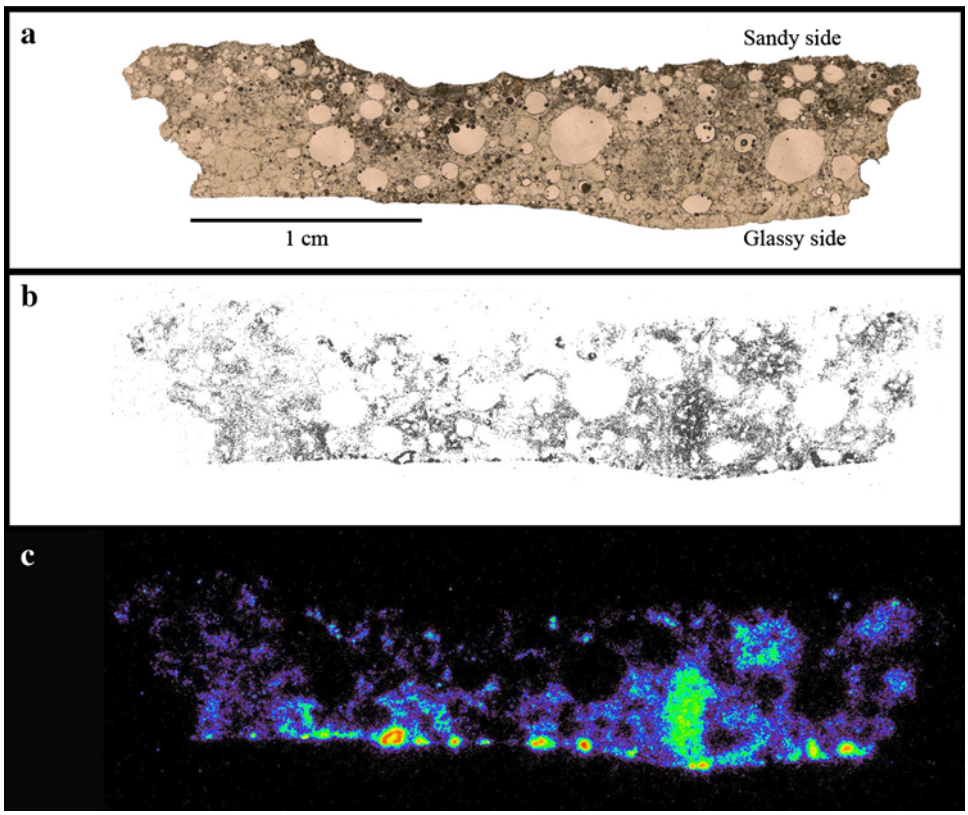

Fig. 2 Optical map of a trinitite thin section (**a**), with corresponding alpha (**b**) and beta (**c**) autoradiographs

in six spots and these indicate a positive correlation with Pu/Zr ratios.

The presence of both ^{152}Eu and ^{154}Eu in trinitite has been documented previously [2, 8], and was verified by γ-spectroscopy (Fig. 1). Calculated δ152/149 versus δ154/149 values are shown in Fig. 5 and are strongly correlated. Enrichments at masses 152 and 154 can be attributed to the presence of ^{152}Eu and ^{154}Eu and/or their decay products. No correlations were identified between δ152/149 or δ154/149 values and Pu/Zr ratios.

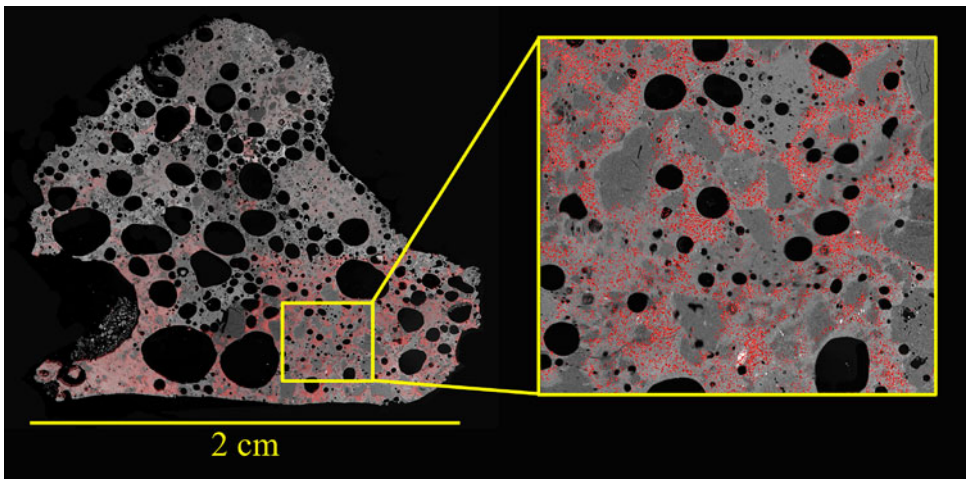

Fig. 3 Back scatter electron (BSE) map of a trinitite thin section with superimposed alpha track radiography map. Contrast in atomic mass (Z) within BSE map is indicated by varying shades of *gray*; lighter areas are indicative of higher Z, which represent the glassy component of trinitite. Remnant Si-rich grains are denoted by *darker gray* (lower Z) areas. *Red color* of alpha map was generated in Photoshop® for contrast against BSE map. Areas of high activity are indicated by increased concentration of *red spots*, and activity is concentrated predominantly within the glassy component (as shown in *inset*)

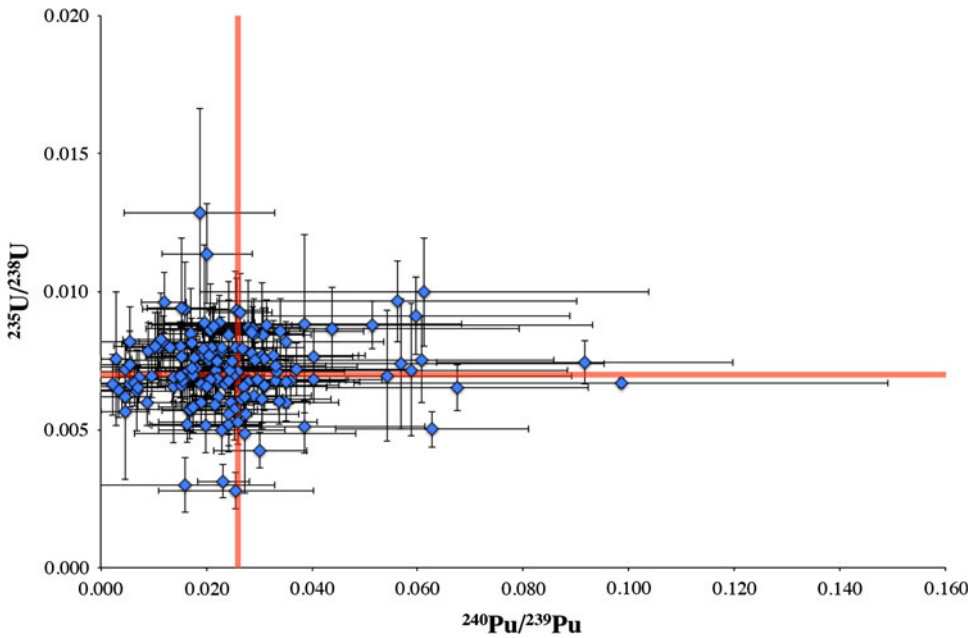

Fig. 4 $^{235}U/^{238}U$ versus $^{240}Pu/^{239}Pu$ for 137 LA-ICP-MS spot analyses of trinitite. The average $^{240}Pu/^{239}Pu$ was 0.0208 ± 0.0012, and the average $^{235}U/^{238}U$ was 0.00718 ± 0.00018

Correlations between Pu and major and trace elements

As the case for Pu, ion signal intensities for all trace elements were normalized to that for Zr. Major element abundances are reported in weight percent oxide values. The relationship between Pu/Zr values and the contents of major and trace elements (e.g., Pu/Zr vs. FeO; Fig. 6) did not reveal correlations for a majority of the analyses (80 out of 98 analyses). The latter are characterized by Pu/Zr ratios ≤0.014 and do not correlate with radionuclide ion signal intensities as well. Conversely, laser ablation spots characterized by Pu/Zr ratios >0.014 do exhibit positive correlations with δ137/138 values (Fig. 7c). Of note, negative trends were observed for Pu/Zr (>0.014) versus SiO_2 and K_2O (Fig. 8).

Discussion

Distribution of alpha and beta activities

The reported distribution of both alpha and beta activities within trinitite is consistent with the formation mechanism proposed by Belloni and supported by Bellucci and Simonetti

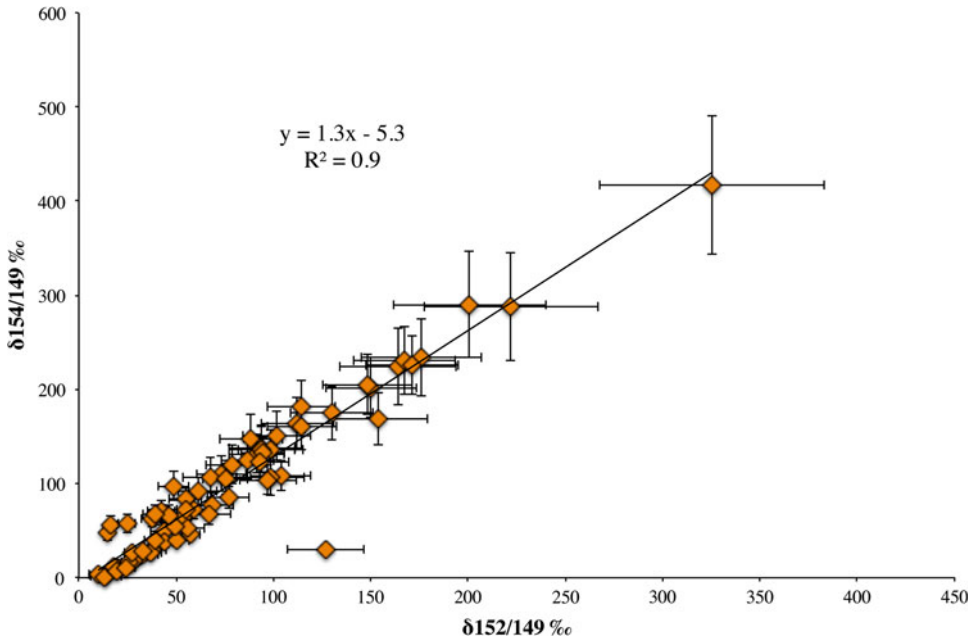

Fig. 5 δ154/149 ‰ versus δ152/149 ‰ for 130 LA-ICP-MS analyses of trinitite

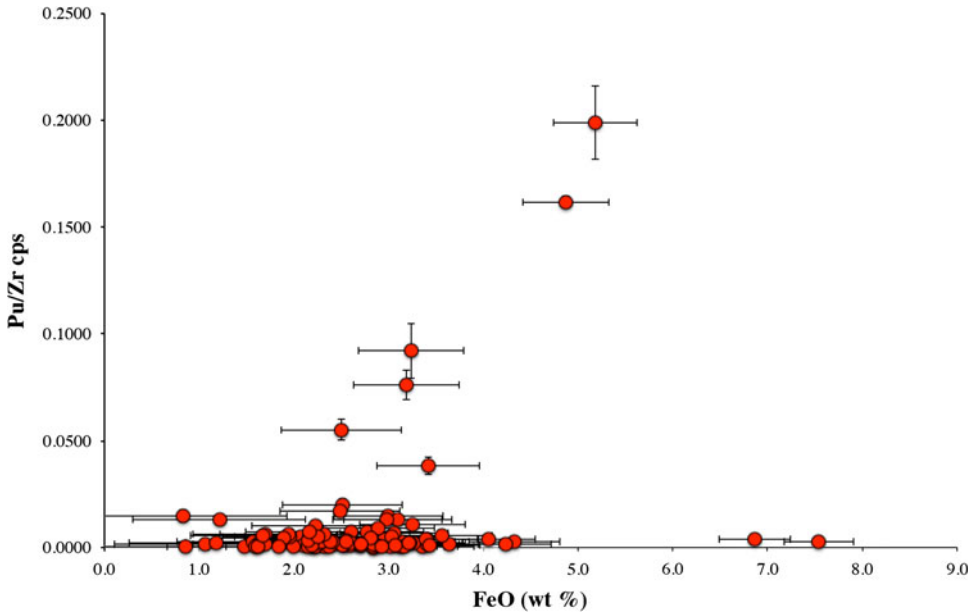

Fig. 6 Pu/Zr cps versus FeO (wt%) for 100 spot analyses of trinitite. Pu/Zr values were determined via LA-ICP-MS, and FeO contents were determined via electron microprobe analysis

[6, 7]. In this process, fission energy from the chain reaction within the Pu core rapidly increased the temperature to $\sim 3 \times 10^7$ K. The core then emitted prompt neutrons, causing neutron activation both within the device components and those from the surrounding desert sand. Subsequently, the emitted thermal energy melted and partially vaporized the sand, and the shock wave from the blast reached the ground, ejecting material into the atmosphere. As the fireball rose, it entrained activated sand. At this point, the liquefied sand left on the ground began to cool and material from the cloud began to condense and rain down on this cooling surface [6, 7]. This formation mechanism resulted in trinitite glass containing low levels of activity throughout each sample, but the majority of the activity is concentrated in and near the glassy surficial layer. This is a result of the condensation of activated particles from the cloud.

According to Eby [4], the majority of mineral phases in the original arkosic sand from which trinitite is derived were melted in the explosion. However, crystalline α-quartz grains are still present. This observation is consistent with our findings, as alpha activity was found to be most concentrated in amorphous phases in between

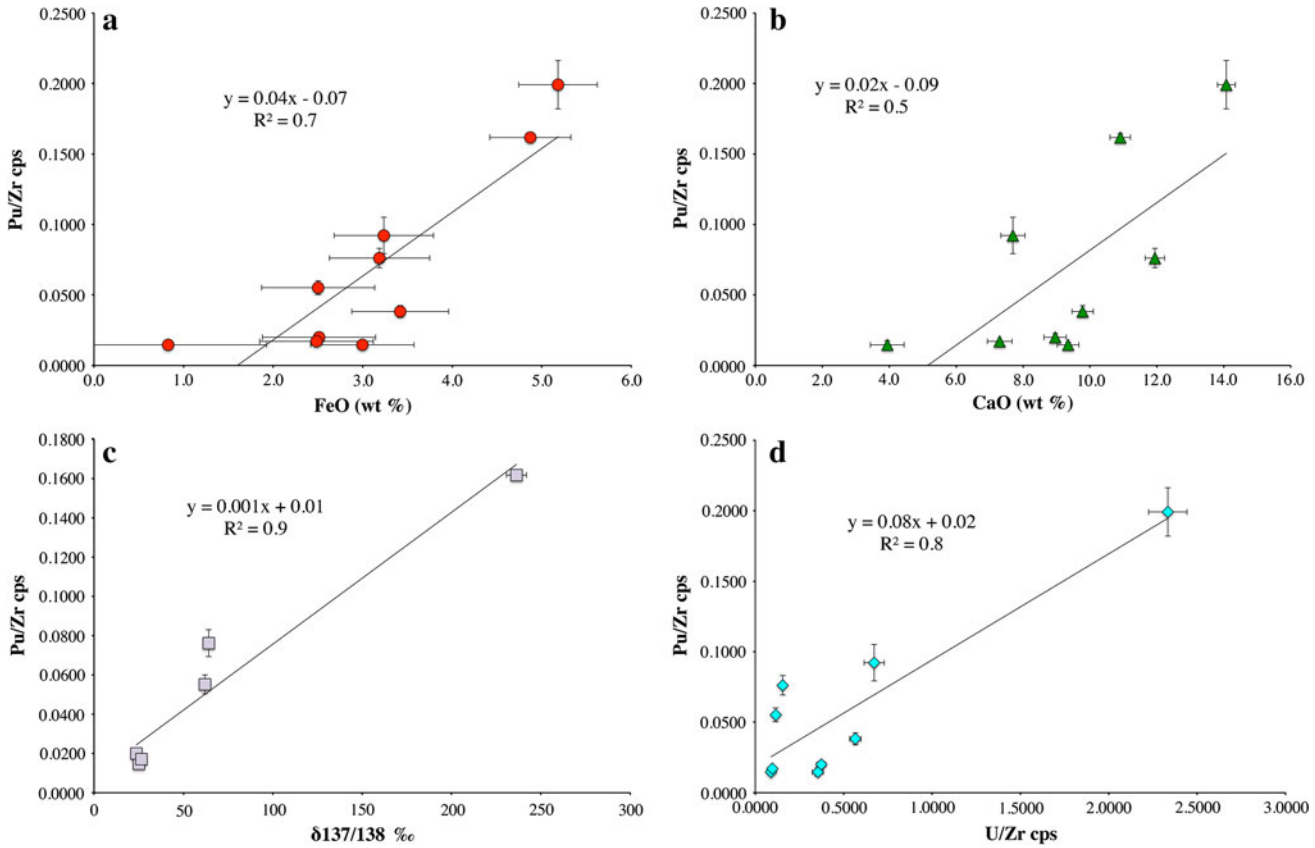

Fig. 7 Pu/Zr versus FeO (**a**), CaO (**b**), δ137/138 ‰ (**c**) and U/Zr (**d**). Only analyses with Pu/Zr values >0.014 are shown

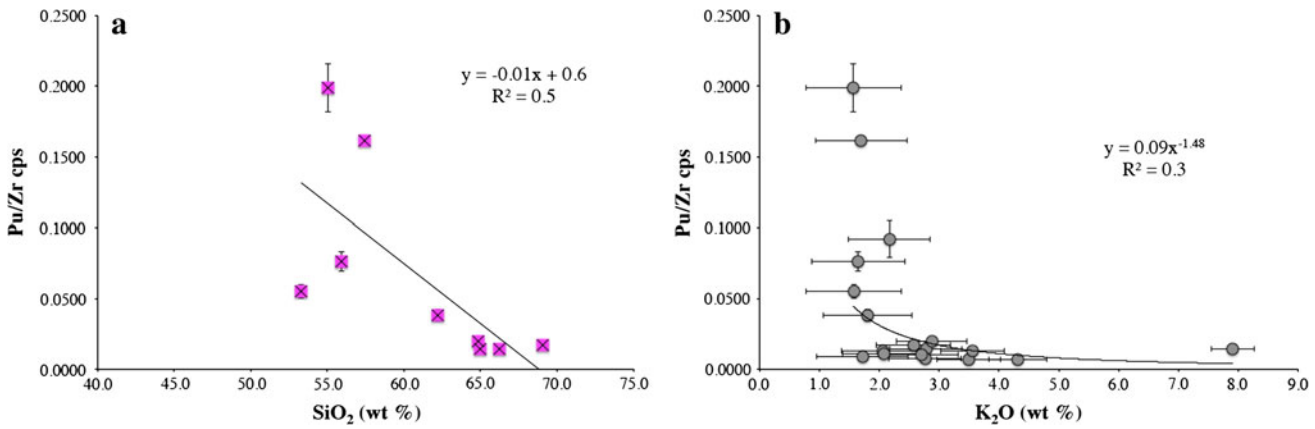

Fig. 8 Pu/Zr versus SiO_2 (**a**) and K_2O (**b**). Only analyses with Pu/Zr values >0.014 are shown

high-Si (presumably quartz) grains or high-Si glass (e.g., Fig. 3). Additionally, LA-ICP-MS results indicate a negative correlation between Pu and SiO_2 wt% contents (Fig. 8). The compositions of these amorphous phases were highly heterogeneous, but typically contained various amounts of Al (0–7 wt%), K (0–3 wt%), Ca (0–9 wt%), Ti (0–10 wt%) Fe (0–30 wt%), Na (0–2 wt%), and Mg (0–3 wt%), in addition to Si. These elements originate from mixing between constituent mineral phases within the arkosic sand, such as K-feldspar, calcite, quartz, and ilmenite [10]. Fahey [11] also noted that alpha activity in trinitite was concentrated within high-Ca areas, which may be attributed to the incorporation of calcite into the melt component. The results from our LA-ICP-MS experiments are also in agreement with these findings (i.e., Fig. 7b).

U and Pu

The $^{235}U/^{238}U$ and $^{240}Pu/^{239}Pu$ ratios measured in this study are shown in Fig. 4. The U isotope ratios are consistent with those for natural uranium, which could derive from both the tamper within the device and natural mineral phases [10]. The average $^{240}Pu/^{239}Pu$ value for the 137 spots measured is 0.0208 ± 0.0012, which differs from the value of 0.0129 ± 0.003 reported in Parekh et al. [2] (as determined via γ-spectrometry). The average value described here is, however, in agreement with the values from Nygren et al. and Douglas [21, 22], and is consistent with "super-grade" Pu (<3 % ^{240}Pu). A ^{240}Pu content of 2.5 % is higher than the Sublette's estimate of 0.9–1.0 % ^{240}Pu in the original fuel [12]. This increase is likely caused by of neutron capture on ^{239}Pu during the explosion. Additionally, the LA-ICP-MS results indicate a strong correlation between U/Zr and Pu/Zr values in areas characterized by higher Pu ion signals (Pu/Zr >0.014; Fig. 7d). This finding supports an association between Pu and U within the device (i.e., from the core and tamper).

Fission and neutron activation products

A positive correlation is noted between δ137/138 and Pu/Zr values (>0.014; Fig. 7c), which indicates the presence of ^{137}Cs and Pu in the same areas within trinitite. Hence, this result spatially links the fuel from the device with one of its fission products. This finding is also consistent with gamma spectroscopy data, in which a positive correlation was observed between ^{137}Cs and ^{241}Am (a derivative of Pu fuel) in bulk trinitite samples [9].

Figure 6 plots δ154/149 versus δ152/149 values and these show a well-defined positive correlation. This result was expected due to the presence and neutron activation of ^{151}Eu and ^{153}Eu to ^{152}Eu and ^{154}Eu within the sand at the test site. No correlation was observed between Pu and ^{152}Eu or ^{154}Eu, which is not surprising as Pu and $^{152,154}Eu$ originate from different sources within trinitite; Pu derives from the device whereas Eu stems from the sand. Bellucci et al. (in press) [8] also reported a lack of correlations between ^{241}Am (derived from Pu fuel) and $^{152,154}Eu$.

Correlations between Pu and major and trace elements

Positive correlations are observed between Pu/Zr (>0.014) values and FeO and CaO contents (Figs. 6, 7). High Fe content in trinitite has been attributed to the iron from the blast tower at ground zero 2, 4, thus it is reasonable that Fe contents correlate positively with Pu ion signals. Similarly, U was present in the device's tamper, and therefore should be correlated with the distribution of Pu within trinitite.

In contrast, negative correlations are identified for Pu/Zr ratios versus SiO_2 and K_2O contents (Pu/Zr >0.014; Fig. 8). This inverse relationship between SiO_2 wt% contents and Pu ion signals is in agreement with the superimposed SEM-BSE results and alpha track radiography data (Fig. 3). The inset of Fig. 3 (image on the right) clearly shows that alpha activity (presumably from U, Pu) is concentrated in the glassy component of trinitite, and is depleted in the crystalline areas. Presumably, some mineral grains were not completely melted in the explosion, and Pu (±U) was unable to incorporate into these phases. Eby 4 found abundant quartz grains in trinitite samples and suggested that it is the predominant mineral in trinitite. Additionally, the negative correlation between Pu/Zr ratios (>0.014) and K_2O contents may be attributed to the presence of K-feldspar crystals in trinitite [10], assuming these did not incorporate Pu (±U) in an analogous fashion to that of quartz.

Conclusions

The results reported here indicate that the distribution of radionuclides within trinitite is highly heterogeneous and complex. We clearly demonstrate here, for the first time, that device-related radionuclides (e.g., U, Pu) are found primarily within the melt (glassy) component of trinitite. In areas characterized by higher Pu ion signals (i.e., abundances), these also contain elevated contents of U and fission products (e.g., ^{137}Cs), which confirm their association with the device. In contrast, crystalline (relatively intact, precursor) mineral phases, such as quartz, K-feldspar, are essentially devoid of radionuclides and other device-related components.

Ideally, a combined approach involving bulk and spatially resolved techniques is recommended for a thorough and accurate forensics assessment of any post detonation debris. Bulk radiochemical analysis is useful for accurate and precise determination of low levels of radionuclides. However, these techniques are time and labor-intensive, and information contained within a spatial context is lost. Additionally, radiochemical analysis cannot be used to determine associations between radionuclides and non-radioactive components of a device. Conversely, LA-ICP-MS requires little sample preparation, and can be used to elucidate some fission products, trace elements, and U and Pu ratios in ~2 min per analysis.

Acknowledgments The authors thank Dr. Ian Steele for his expertise with electron microprobe analysis. Sandy Dillard of the Brazos Valley Petrographic Thin Section Services Lab (Bryan, Texas) is thanked for the production of high quality thin sections of trinitite. Lastly, the authors thank Bruce McNamara, Frances Smith, Rachel Lund, and Judah Friese at Pacific Northwest National Laboratory for

assistance with beta radiography. We are appreciative of the insightful comments provided by two anonymous reviewers. This research work was funded by DOE/NNSA Grant PDP11-40/DE-NA0001112.

References

1. United States Department of Energy Nevada Operations Office (2012) United States Nuclear Tests July 1945 through September 1992 2000. 185
2. Parekh P, Semkow T, Torres M, Haines D, Cooper J, Rosenberg P, Kitto M (2006) Radioactivity in Trinitite six decades later. J Environ Radioact 85:103–120
3. Rhodes R (1986) The making of the atomic bomb: Simon and Shuster
4. Eby N, Hermes R, Charnley N, Smoliga JA (2010) Trinitite—the atomic rock. Geol Today 26:180
5. Storms B (1965) The Atom. In: Trinity. University of California, Los Alamos Scientific Laboratory, Office of Public Relations, Los Alamos, p 1
6. Belloni F, Himbert J, Marzocchi O, Romanello V (2011) Investigating incorporation and distribution of radionuclides in trinitite. J Environ Radioact 102:852–862
7. Bellucci JJ, Simonetti A (2012) Nuclear forensics: searching for nuclear device debris in trinitite-hosted inclusions. J Radioanal Nucl Chem 293:313–319
8. Bellucci JJ, Wallace C, Koeman EC, Simonetti A, Burns PC, Kieser J, Port E, Walczak T (in press) Distribution and behavior or some radionuclides in the Trinity nuclear test. J Radioanal Nuclear Chem
9. Salter L, Harley J (1965) Trinitite—Cobalt-60 Cesium-137 and Europium-152. Science 148:954
10. Bellucci JJ, Simonetti A, Wallace C, Koeman EC, Burns PC (2012) Geochemistry of the Trinity nuclear test: investigation of Trinitite glass at high spatial resolution. 39th Annual Meeting of FACSS: SciX Conference Abstracts. p 119
11. Fahey AJ, Zeissler CJ, Newbury DE, Davis J, Lindstrom RM (2010) Postdetonation nuclear debris for attribution. Proc Natl Acad Sci USA 107:20207–20212
12. Sublette C (2012) Nuclear weapons frequently asked questions 2001
13. Glasstone S, Dolan PJ (1977) The effects of nuclear weapons. US Department of Defense, US Energy Research and Development Agency, Washington, D.C.
14. Widner T, Shonka J, Burns R, Flack S, Buddenbaum J, O'Brien J, Robinson K, Knutsen J (2009) Final report of CDC's LAHDRA project
15. Semkow TM, Parekh PP, Haines DK (2006) Modeling the effects of the Trinity test. In: Applied modeling and computations in nuclear science: American Chemical Society, p 142
16. Wahl A (1988) Nuclear-charge distribution and delayed-neutron yields for thermal-neutron-induced fission of U-235, U-233 and Pu-239 and for spontaneous fission of Cf-252. At Data Nucl Data Tables 39:1–156
17. Chen W, Simonetti A (2012) In-situ determination of major and trace elements in calcite and apatite, and U-Pb ages of apatite from the Oka carbonitite complex: insights into a complex crystallization history. Chem Geol. doi:10.1016/j.chemgeo.2012.04.022
18. Boulyga S, Tibi M, Heumann K (2004) Application of isotope-dilution laser ablation ICP-MS for direct determination of Pu concentrations in soils at pg g(−1) levels. Anal Bioanal Chem 378:342–347
19. Vertes A, Nagy S, Kencsar Z (2011) Intstrumentation, separation techniques, environmental issues. In: Handbook of nuclear chemistry. Springer, p 2491
20. Ludwig KR (2003) User's manual for isoplot 3.00 a geochronological toolkit for Microsoft Excel
21. Nygren U, Rameback H, Nilsson C (2007) Age determination of plutonium using inductively coupled plasma mass spectrometry. J Radioanal Nucl Chem 272:45–51
22. Douglas RL (1978) Levels and distribution of environmental plutonium around the Trinity site; ORP/LV-78-3